Research Article

Adsorption Thermodynamics, Modeling, and Kinetics Studies for the Removal of Lead Ions Using ZnO Nanorods

Sadia Ata,[1] **Anila Tabassum,**[1] **Ifra Shaheed,**[1] **Ijaz ul Mohsin,**[2] **Norah Alwadai** ⬤,[3]
Maryam Al Huwayz ⬤,[3] **Munawar Iqbal** ⬤,[4,5] **and Arif Nazir** ⬤[5]

[1]*School of Chemistry, University of the Punjab, Lahore, Pakistan*
[2]*Institute for Applied Materials–Applied Materials Physics (IAM-AWP), Karlsruhe Institute of Technology, Karlsruhe, Germany*
[3]*Department of Physics, College of Sciences, Princess Nourah bint Abdulrahman University, P.O. Box 84428, Riyadh 11671, Saudi Arabia*
[4]*Department of Chemistry, Division of Science and Technology, University of Education, Lahore, Pakistan*
[5]*Department of Chemistry, The University of Lahore, Lahore, Pakistan*

Correspondence should be addressed to Arif Nazir; arif.nazir@chem.uol.edu.pk

In the present investigation, zinc oxide nanorods (ZnO-NR) were synthesized via the hydrothermal method using $ZnCl_2$ as a zinc ion precursor in the presence of cetyltrimethylammonium bromide. Synthesized ZnO-NR was featured using advanced techniques including XRD, PL, SEM, and UV-visible spectroscopy. The role of these assynthesized ZnO-NR was evaluated for the sequestration of lead ions in batch mode. The elimination of lead ions was achieved at pH 6-7 using a 0.06 g adsorbent dose, 25 min contact time, 25 mg/L initial lead ion concentration, 323 K temperature, and 200 rpm agitation speed. A thermodynamic study revealed the endothermic nature of lead ion sequestration onto ZnO-NR. The lead ion sequestration followed kinetic (pseudo-second-order) and isotherm (Langmuir) models. The lead ions were eliminated up to 142 mg/g at the optimum level of affecting variables. The ZnO-NR might be a potential adsorbent for lead ion removal from industrial effluents.

1. Introduction

Nanomaterials have tremendous applications in environmental challenges, including medicines, catalysis, water treatments, and solar energy conversion [1–3]. Numerous researchers in the field of nanoparticle synthesis believe that metal oxides are much better agents for cleaning or purifying the environment. This can be attributed to their ability to act as an efficient adsorbent for pollutants. The aforementioned ability is associated with their greater surface area-to-volume ratio. For example, different metal oxide nanomaterials (Fe_2O_3, CeO_2, Al_2O_3, TiO_2, MnO_2, NiO, ZnO, and MgO) have shown their character for the sequestration of metallic ions from wastewater.

The environmental pollution caused by lead ions has tremendously increased due to industrialization and is considered a severe health hazard. Exposure to Pb(II) leads to nervous system damage, anemia, mental retardation, renal kidney disease, and cancer. Mining, plumbing, painting and printing processes, petroleum industries, and automobile batteries are the major sources of contamination. Different world agencies, e.g., USEPA and WHO have set the maximum allowed Pb levels (0.015 mg/L and 0.01 mg/L), respectively, in potable water [4]. So, the matter is of great concern, and there is a need to remove lead from water. There are many methods used to remove Pb from water, e.g., solvent extraction, ion-exchange membranes, chemical precipitation, adsorption, and membrane separation [5–8]. Among these terminologies, adsorption is considered viable because of the availability of different adsorbents, easy handling, high efficiency, and recycling of the adsorbed metal ions [9].

Zinc oxide (ZnO) is an *n*-type semiconducting material, exhibits excitation binding energy (60 m eV), and has been applied in various applications (solar cells, biosensors, gas sensors, nanogenerators, varistors, photocatalysts, and

photodetectors) [10]. ZnO nanostructures like nanowires, nanorods, nanotubes, and nanobelts were prepared and employed in different fields. Sol-gel, hydrothermal, thermal decomposition, precipitation, ultrasonication, microemulsion, pyrolysis, electrodeposition, chemical vapor deposition, and microwave-assisted techniques have been successfully used for ZnO-NR fabrication [11]. Moreover, the synthesized NR stability, crystal growth control, sizes, morphologies, and distribution also need to adopt a specific method. On the other hand, green chemistry demands ecobenign methods for the fabrication of nanomaterials. Plant materials have emerged as an eco-friendly alternative to synthetic chemical methods.

The hydrothermal method has gained much attention due to its simple apparatus, catalyst-free reaction, controlled particle size, environmental friendliness, and cost-effectiveness. The conditions for hydrothermal reaction at high temperature (100–300°C) and pressure in an aqueous medium are employed, and in response to heating followed by cooling at room temperature, crystal nuclei are produced and grown. The morphology of these crystal nuclei is greatly influenced by the composition of the reaction mixture, concentration of reactants, and temperature and pressure of the reaction media which results in a product having a high degree of crystallinity as well as high purity [12].

A hydrothermal approach was used for the fabrication of ZnO-NR. Then, the efficiency of this synthesized ZnO-NR was appraised for the removal of lead ions. Various operational variables, i.e., adsorbent amount, pH, reaction time, temperature, shaking speed, and initial concentration, were optimized and performed systematically in a batch process. Isotherm modeling, kinetics, and thermodynamics were analyzed to comprehend the process of lead removal using synthesized ZnO-NR.

2. Material and Methods

The chemicals were procured from Merck (Germany). The $Pb(NO_3)_2$ 1000 mg/L solution was prepared, and dilutions were made for further use. To prevent hydrolysis, 1% of HNO_3 was added. Different working solutions of varying concentrations were arranged using distilled water.

2.1. Synthesis Protocol. The hydrothermal method in the presence of cetyltrimethylammonium bromide (CTAB) was employed for the preparation of ZnO-NR. The $ZnCl_2$, NaOH, and CTAB solutions in water were mixed in a molar ratio of 1 : 2 : 1. The mixture was agitated vigorously for 10 min and transferred to an autoclave cell having a Teflon chamber. Then, the content was heated at 180°C for 3 h, cooled down to 25°C, and centrifuged at 3000 rpm (20 min) to discrete the precipitates from the mixture. Then, these obtained white ppt. and were washed with methanol and distilled water several times. This washing continues until pH 7 was achieved. Then, ppt. was kept in an oven at 80°C for 4 h [13].

2.2. Characterization of Nanorods. UV-visible spectrum was taken on PG-T 90$^+$ Double Beam UV-VIS Spectrophotometer. The data was achieved in 340-400 nm. Bruker D 8 dif-

fractometer was employed for XRD analysis. The other conditions are Cu Kα, have $\lambda = 1.5406$ Å radiations at 45 kV and 40 mA with a scanning angle (2θ) of 20°–80° and the scanning rate is 0.038 s^{-1} with a step time of 3 s. The photoluminescence (PL) spectrum was measured using F2500 FL-Spectrophotometer, Hitachi.

2.3. Batch Run Protocol. A batch mode of analysis was used for the lead ion removal using ZnO-NR. The ZnO-NR and 50 mL of lead ion solution (50 mg/L) were mixed and subjected to shaking for an appropriate time. The influences of adsorbent dose, initial concentration of lead ions, pH, reaction time, temperature, and agitation speed were studied. The metal ion solution and adsorbent were mixed for a programmed time interval. The resultant solution was a suspension, which was centrifuged for 20 min at the rate of 3000 rpm. The influence of the dose of adsorbent was evaluated by mixing different quantities of adsorbent (0.02-0.20 g) with lead ion solution (50 mg/L, 50 mL). The mixture was stirred for 30 min at 200 rpm at 25°C. The pH effect was studied by the variations in the pH of the solution from pH 3 to pH 8, which was adjusted using 0.1 MHNO_3/NaOH. 50 mL of the solution was mixed with 0.06 g of adsorbent and subjected to shaking at 200 rpm for half an hour at 25°C. For the contact time study, a 0.06 g of adsorbent was assorted with 50 mL of the solution and stirred at 200 rpm, and contact time was studied in 0-30 min range at pH 6 and 25°C. The effect of initial metal ion concentrations was studied by shaking 0.06 g of adsorbent with 50 mL of lead ions solution. This was performed by varying initial concentrations of 50-500 mg/L at an agitation rate of 200 rpm at pH 6, 25°C for 30 min. To find out the impact of temperature, 0.06 g of ZnO-NR was assorted with a lead solution and temperature was varied between 293 and 323 K. The AAS was used for the residual concentration of lead ions determined. All the trials were conducted in thrice and data was averaged. The removal efficiency (percentage removal and q_e, mg/g) were computed as depicted as follows:

$$\text{Removal (\%)} = \frac{(C_o - C_e)}{C_o} \times 100,$$
$$q_e = (C_o - C_e)\frac{V}{W}, \tag{1}$$

where C_0, C_e, V, and W are the lead ions at time "0" and at time "t", volume (L), and adsorbent dose (g).

3. Results and Discussion

3.1. Properties of ZnO Nanorods. Ultraviolet-visible analysis is useful to evaluate the light absorption nature of the materials [14], which results in the excitation of the electrons from lower to higher energy levels. The UV-visible spectrum of ZnO-NR dispersed in distilled water is presented in Figure 1. There appears to be a strong peak in the UV-visible spectrum at 375 nm. This could be the start of the visible region or the end of the UV region depending on the type of instrumental conditions. This peak is linked with the band gap of ZnO-NR, and the reason for this peak can
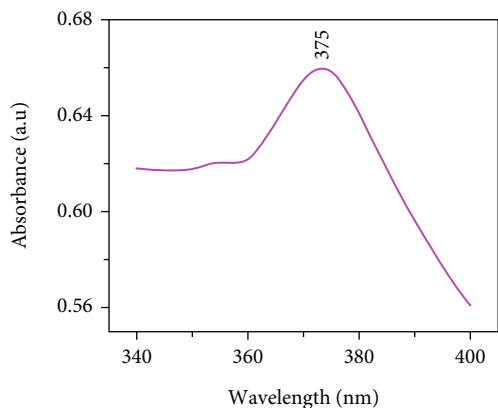
Figure 1: UV-visible analysis ZnO-NR prepared via hydrothermal route.

Figure 2: ZnO-NR (prepared via hydrothermal route) band gap energy.

also be linked with the electronic transition between the valence and conduction bands [15]. The peak shifts towards the shorter wavelength with reference to the bulk ZnO band edge [16]. This kind of blue shift could be linked with a change in the particles' size [17, 18]. It has been observed that the absorption edge moves towards a short wavelength when particle size reduces as compared to its bulk counterpart, and hence, its band gap energy values increase [19]. The Tauc relationship (Equation (2)) is employed for band gap estimation.

$$\alpha h v^n = B (h v - Eg), \qquad (2)$$

where hv equals energy and α is the coefficient of absorption. The letter B exhibits constant, n is considered 1/2 for semiconductor direct band gap estimation, and Eg stands for band gap energy. The linear part of the graph could be extrapolated to calculate the band gap energy, as shown in Figure 2. The band gap energy (3.38 eV) was calculated using the absorption data.

The structural and phase analyses were performed by XRD analysis [20], and the response is portrayed in Figure 3. The XRD diffraction peaks confirmed the presence of hexagonal wurtzite-structured ZnO (JCPDS Card. 36-1451). In addition, the peaks are quite intense and sharp, suggesting that the particles are highly crystalline. No peak corresponding to other impure phases is observed, indicating the purity of the sample. The Debye–Scherrer equation is employed for the monitoring of crystallite size.

$$D = \frac{K\lambda}{\beta \cos \theta}, \qquad (3)$$

where D, K, λ, θ, and β are presenting the grain size (nm), constant (0.89), X-ray wavelength (1.54 Å), and FWHM, respectively. The spectrum revealed an intense peak corresponding to plane 101, and the particle size was ~19 nm.
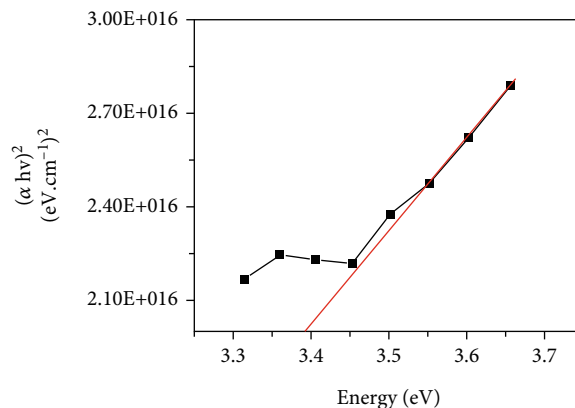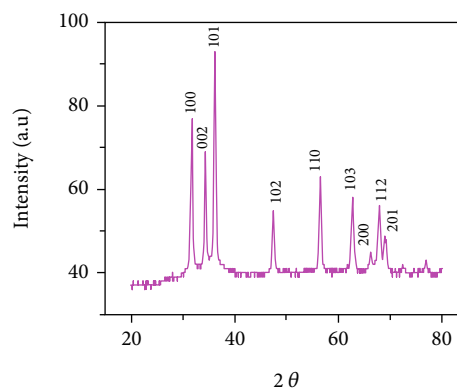

Figure 3: XRD analysis of ZnO-NR prepared via hydrothermal route.

The morphology was studied by SEM analysis [21], and Figure 4 exhibits the SEM image of prepared ZnO-NR. The images clearly revealed a spongy mass of rod-like structures with a 60-70 nm particle size. The structure has pores that facilitate the adsorption of lead. Figure 5 depicts the photoluminescence (PL) spectrum of ZnO-NR. The spectrum revealed two emission bands, one corresponding to UV emission at 397 nm and the second is a broad visible emission at 590 nm. The UV emission is usually correlated with the transfer of photon generated from the CB to the VB. The response thus observed illustrated the trapping of electrons and holes by defects present in the sample. This trapping of electrons and holes further hindered their recombination and thus improved the photocatalytic properties of semiconductor materials. The defects in the visible region are generally arisen due to the doping or impurities present in the sample. In ZnO, these defects are related to interstitial defects of oxygen and zinc, vacancies in oxygen and zinc, oxygen substitution at zinc, and complex of oxygen vacancy with zinc interstitial. Moreover, the peak intensity of UV emission is related to the crystalline nature of the sample. While the visible emission peak intensity depicted the defects are present in the sample. Thus, the analysis of the spectrum shows that the fabricated ZnO-NR is crystalline in nature with defects.
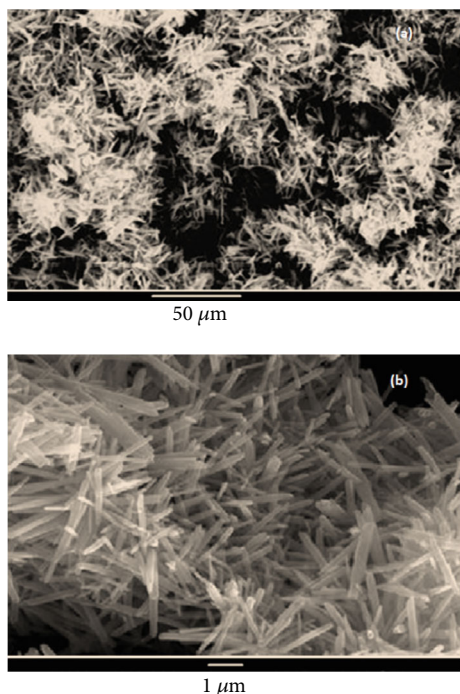
FIGURE 4: SEM analysis of ZnO-NR prepared via hydrothermal route at different resolutions, (a) 50 μm (b) 1 μm.
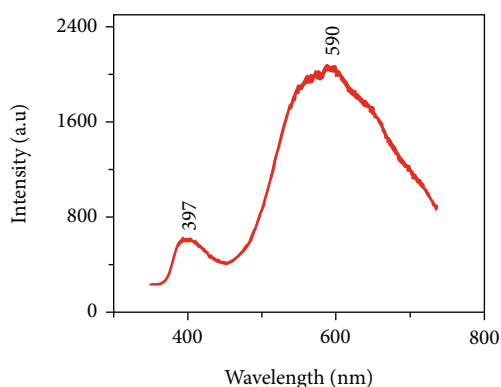

FIGURE 5: Photoluminescence spectrum of ZnO-NR prepared via hydrothermal route.

3.2. Pb Ion Removal Performance

3.2.1. Adsorbent Dose Impact.
The sequestration process of metal ions on NPs is dependent on adsorbent dosage (Figure 6). By increasing the adsorbent dosage, lead ion removal was significantly increased. It is revealed that sequestration depends on the active moieties on the adsorbent surface, and a certain quantity of adsorbent enhanced the sequestration capacity of the adsorbent. After a certain point, the adsorbent dose effect became insignificant at an extremely higher adsorbent dose, and removal efficiency did not change. This is further ascribed to the saturation of the active moieties on the adsorbent surface. This point is called the equilibrium point, where the number of ions in aqueous media and the amount of ions on the solid
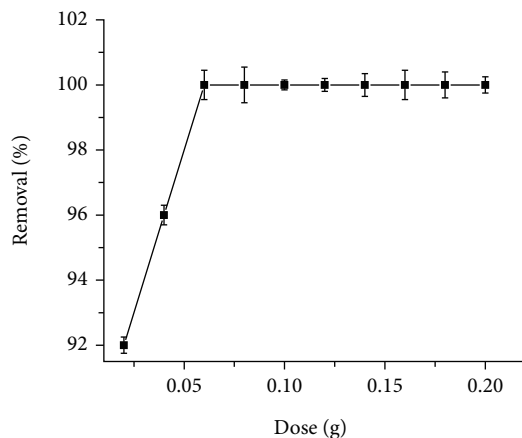

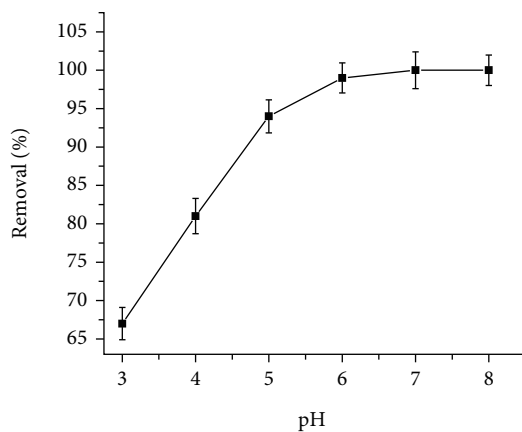FIGURE 6: Lead ions removal (%) versus ZnO-NR dose.

FIGURE 7: Lead ions removal (%) versus pH using ZnO-NR.

surface become constant [22]. In our experiment, the maximum percentage sequestration of lead ions was obtained with an adsorbent dosage of 0.06 g.

3.2.2. pH Influence.
The pH of the metal ion solution exerts a profound effect on the process of sequestration as it influences metal ion solubility and adsorbent ionizing ability. As shown in Figure 7, when the pH value was low (<7), the hydrogen ion concentration increases; thus, there is a struggle between H^+ and Pb^{2+} for the same active site, which results in lower sequestration efficiency. While at higher pH (>7), hydrolysis and precipitation of metal ions are started. Therefore, the percent removal remained constant above pH 7. In a pH range of 7-11, different species of Pb(II), i.e., $Pb(OH)_2$ and $Pb(OH)^+$ are prominent, which in turn furnished higher percentage sequestration of lead ions by sequestration of ($Pb(OH)^+$) and precipitation of ($Pb(OH)_2$). The influence of the pH of the solution on the removal process can also be elucidated on the basis of two factors. These could be charges on the adsorbent surface and adsorbate speciation. The adsorbent surface at lower pH acts as a hydrous oxide and is covered by hydrogen ions (MOH^{+2}). On the other hand, deprotonated oxide (MO^-) is produced by hydroxyl ions by reacting with the hydrous oxide under
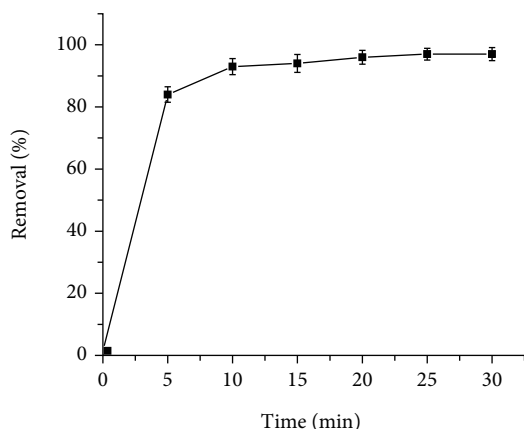
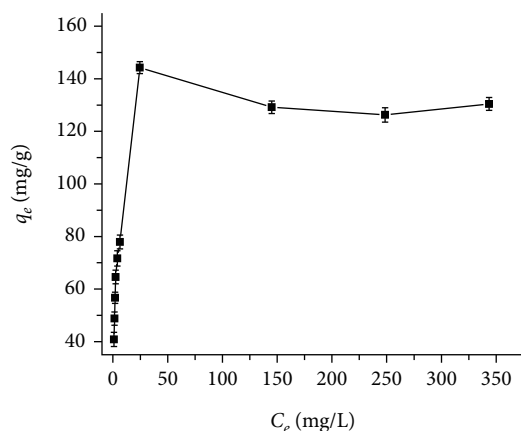FIGURE 8: Lead ions removal (%) versus contact time using ZnO-NR.

FIGURE 9: Lead ions removal (%) versus lead ions initial concentration using ZnO-NR.

FIGURE 10: Lead ions removal (%) versus temperature using ZnO-NR.

basic condition. This will interact with metal cation and lead to more sequestration [23]. The sequestration capacity was low at a lower pH (in an acidic region). On the other hand, when pH increased from 4 to 5, the percentage sequestration of lead ions increased significantly. The maximum adsorbent was in pH 6-7 range. These results revealed that the pH of the solution has a remarkable impression on the sequestration mechanism of lead ions. Thus, the optimum pH value is determined to be 6.0 for maximum lead ion sequestration.

3.2.3. Contact Time Influence. Adsorption is a time-dependent phenomenon, and the effect of contact time on lead ion sequestration on ZnO-NR was also investigated, and the response is presented in Figure 8. Initially, the sequestration rate was fast at the initial stage, which braked in the second phase, and then was equilibrium reached in half an hour (30 min). The number of active sites was higher initially, which binds the metal ions favorably. Later, the rate of sequestration slowed down, due to the coverage of binding sites present on the surface, and the sequestration did not change considerably beyond this time [24].

3.2.4. Initial Concentration Influence. The lead ion sequestration efficiency of ZnO-NR for different concentrations is depicted in Figure 9. The increased metal ion concentration also enhanced the sequestration process of ZnO-NR. At higher metal ion concentrations, the active sites are surrounded by a large number of metal ions, which facilitates the sequestration of lead ions. On the contrary, the percentage sequestration of lead ions was declined as the initial metal ion concentration was increased. At lesser concentration, the surface of ZnO was unsaturated, but as the concentration increased, the surface becomes drenched with lead ions and thus, limits the removal capacity of the adsorbent. Therefore, higher concentration results in lower percentage elimination of the lead ions, which reveals that the sequestration of lead ions was dependent on initial concentration [25].

3.2.5. Temperature Influence. The impact of temperature on the sequestration capacity of lead ions on ZnO-NR was studied in the 293-323 K range, and the responses thus observed are depicted in Figure 10. It can be seen that as the temperature increased, the sequestration efficacy of the lead ions was also increased, which is an indication of an endothermic sequestration nature process [22]. When temperature is increased, the mobility of metal ions increased, resulting in effective interaction between binding sites and lead ions, leading to improve the sequestration of lead ions with temperature.
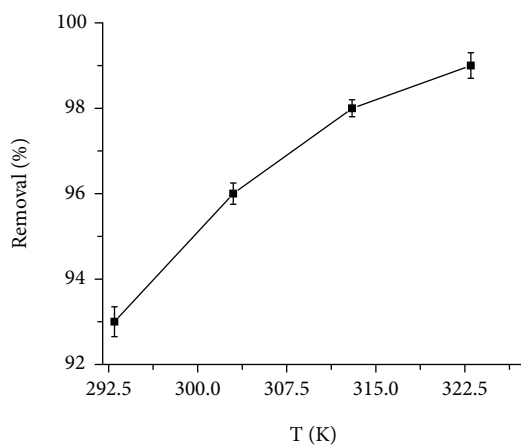
3.2.6. Agitation Influence. The agitation of the adsorbent and adsorbate may also influence the sequestration efficiency, which was also studied for the sequestration of lead ions. The agitation effect was studied in the 100-260 rpm range, and the response is presented in Figure 11. It was observed that as the agitation speed increased, the sequestration efficacy of the lead ions was also increased and was maximum at 200 rpm. After 200 rpm agitation speed, there was no change in sequestration. It has been reported that agitation provides forces that collapse the adsorbent agglomerates and generate a well-dispersive system, which resultantly affects the sequestration of the adsorbate on the adsorbent. The agitation also properly distributes the adsorbent throughout the bulk solution.
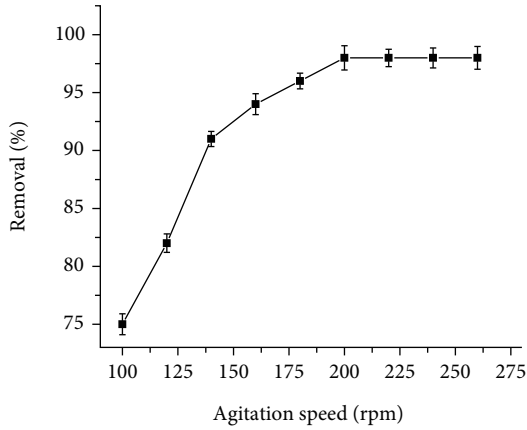
FIGURE 11: Lead ions removal (%) versus agitation speed using ZnO-NR.

TABLE 1: Adsorption isotherm parameters for the adsorption of Pb(II) ions onto ZnO nanorods.

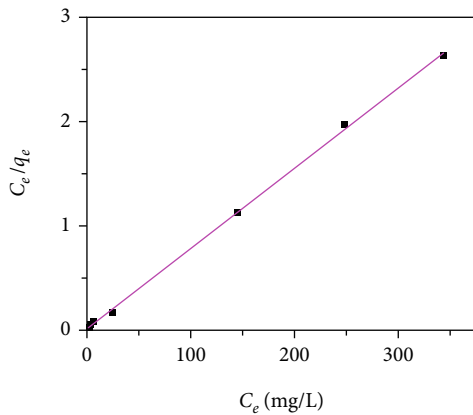| Isotherm model	Parameters calculated
Langmuir's isotherm	
q_m (mg/g)	142
K_L (L/mg)	0.4046
R^2	0.9994
Freundlich isotherm	
K_F (mg/g)	51.008
n	5.3219
R^2	0.8076

FIGURE 12: Langmuir's isotherm plot for the removal of lead ions using ZnO-NR.

3.3. Adsorption Isotherm Modeling.

Adsorption isotherms give an insight into how adsorbate interacts with the adsorbent as a function of concentration. The results obtained by these isotherms help in finding the maximum sequestration capacity [26, 27]. The most commonly used isotherms for understanding the adsorption process include Freundlich and Langmuir.
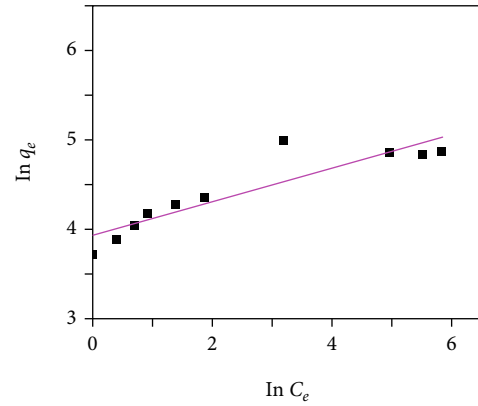

FIGURE 13: Freundlich's isotherm plot for the removal of lead ions using ZnO-NR.

TABLE 2: Kinetic parameters for the adsorption of Pb(II) ions onto ZnO.

Kinetic equation	Parameters calculated
q_e (theory)	40.416
Pseudo-first-order	
k_1 (/min)	0.563
q_e (cal) (mg/g)	270.96
R^2	0.7577
Pseudo-second-order	
k_2 (g/mg/min/)	0.0251
q_e (theory) (mg/g)	43.47
h	47.4299
R^2	0.9998
Intraparticle diffusion	
k_{id} (mg/g/min$^{1/2}$)	6.8903
R^2	0.7133

Langmuir's model presumes the adsorption as a monolayer formation, and binding sites are homogeneous and equivalent energetically, also, one ion is an adsorbent/binding site [28]. The Langmuir model is expressed as follows:

$$\frac{C_e}{q_e} = \frac{C_e}{q_m} + \frac{1}{K_L q_m}, \tag{4}$$

where C_e, q_m, and q_e indicate the concentration (equilibrium), the sequestration efficacy, and sequestration at equilibrium, respectively. The k_L is the constant (L/mg) which is related to the sequestration energy coefficient. The plot of C_e/q_e against C_e would result in a straight line for model validity. The sequestration capacity and energy be calculated from the slope and intercept of the plot. Related to the Langmuir isotherm, R_L (separation factor) is depicted in the following:

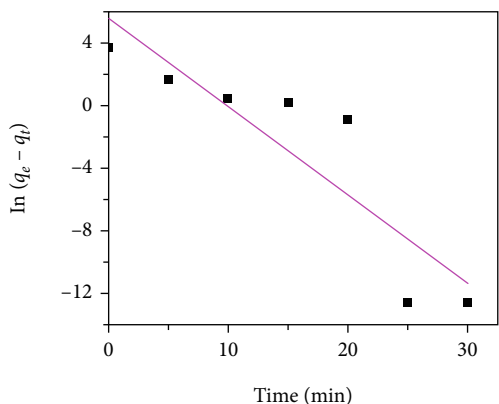$$R_L = \frac{1}{1 + K_L C_0}, \tag{5}$$

FIGURE 14: Kinetics plot (pseudo-first-order) for the removal of lead ions using ZnO-NR.
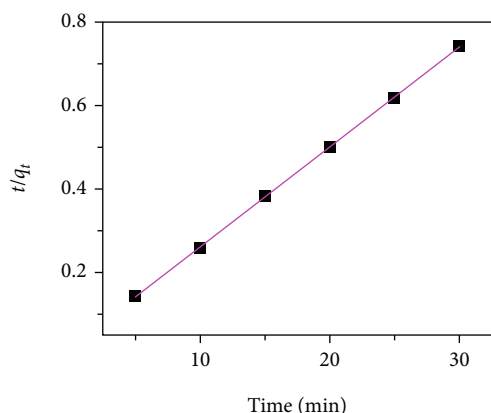

FIGURE 15: Kinetics plot (pseudo-second-order) for the removal of lead ions using ZnO-NR.
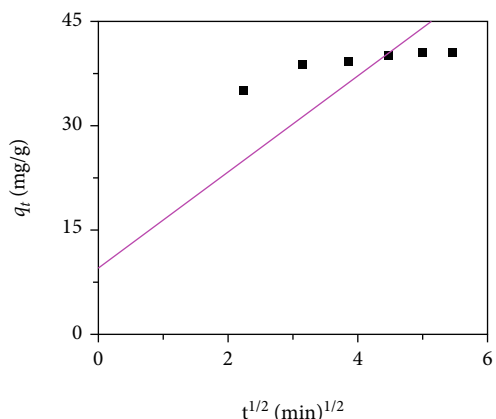

FIGURE 16: Intraparticle diffusion plot for the removal of lead ions using ZnO-NR.

where C_o and R_L present lead ion initial concentration and isotherm shape, respectively; $R_L = 0$ (irreversible); $R_L = 1$ (linear); and if $R_L > 1$ (unfavorable) [29]. The R_L values calculated for lead ions are in 0.046-0.0048 range for 50-500 mg/L initial lead ions. The values are greater than zero but less than one. This indicates that ZnO-NR is considered appropriate material for lead ion sequestration.
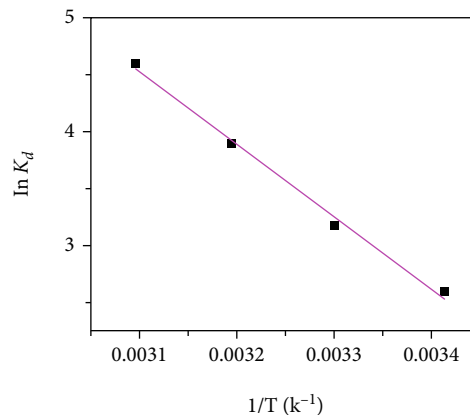

FIGURE 17: $\ln k_D$ versus 1/T plot for the removal of lead ions using ZnO-NR.

TABLE 3: Thermodynamic parameters for the adsorption of Pb(II) ions onto ZnO.

Temperature (K)	$\Delta G \circ$ (kJ/Mol)	$\Delta H \circ$ (kJ/Mol)	$\Delta S \circ$ (J/K Mol)
293	-2.53543	75.61	0.258
303	-8.43365		
313	-21.0548		
323	-51.023		

The Freundlich model undertakes multilayer formation on nonuniform active sites on the adsorbent surface and linear relation is depicted in the following [30]:

$$\ln q_e = \ln K_f + \frac{1}{n} \ln C_e, \tag{6}$$

where K_f and $1/n$ are the Freundlich constants. The K_f and n stand for sequestration capability and energy distribution. The linear process of sequestration is indicated by the value of n equals unity. Anything less than unity indicates a chemical process while more than unity expresses the physical process for sequestration. If Freundlich's isotherm model has been followed then the plot of $\ln q_e$ against $\ln C_e$ (slope = $1/n$ and intercept = $\ln K_f$. The calculated parameters for both isotherms are portrayed in Table 1 and Figures 12 and 13. It is concluded from the data attained that the experimental results are well suited to the Langmuir isotherm model. This was associated with a high regression coefficient of 0.999 versus Freundlich's model. So, it indicates a monolayer of lead ions that are and uniformly sequestration on to ZnO-NR surface [31].

3.4. Kinetics Studies. Adsorption is a time-dependent phenomenon. The impact of contact time on lead ion sequestration to ZnO-NR is studied to evaluate the sequestration kinetics. Results revealed that the rate of sequestration was much fast initially until the equilibrium is established. There are large numbers of active sites present at the start. This richness of exchangeable sites favors the binding of lead ions to the

TABLE 4: Lead ions removal using various nanoadsorbents and nanocomposites.

S. no	Adsorbent	Adsorption
1	γ-Fe$_2$O$_3$	50
2	Fe$_3$O$_4$@SA–Zr	333.33
3	γ-Fe$_2$O$_3$	71.42
4	Fe$_3$O$_4$	79.3
5	Magnetite–hematite	617.3
6	Fe$_3$O$_4$	36
7	Fe$_3$O$_4$	76.8
8	Fe$_3$O$_4$	46.18
9	γ-FeOOH	527.944
10	α-FeOOH	820.165
11	G-nZVI	97
12	AF-Fe$_3$O$_4$	369
13	Fe$_3$O$_4$-DMSA	-99
14	NH$_2$-HCMSSs	194.3
15	CoFe$_2$O$_4$–NH$_2$	140.1
16	NiO (25 nm)	62.5
17	NiO (28 nm)	625
18	NiO (38-130 nm)	50.505
19	CuO	160.7
20	ZnO	26.109
21	Si–OH & Al–OH	100
22	TiO$_2$	132.458
23	Ti-AM	476.19
24	MnOs	80.1
25	Hydrated MnOs	204.1
26	Si	83.3
27	XG-g-PAM/SiO$_2$	537.634
28	Fe$_3$O$_4$/silica–XG	21.32
29	SiOH	46.3
30	Si	200.8
31	SWCNTs/WSh	185.2
32	Fe$_3$O$_4$-GS	27.95
33	PAS-GO	312.5
34	PoPD/RGO	228
35	HFO-001, TiP-001, HMO-001	395
36	CS-TPP	398
37	CS-MAA	11.3
38	HAP	1429
39	CS/Fe-HAP	1385
40	SiO$_2$-nH$_2$O	60
41	γ-Fe$_2$O$_3$	68.9
42	SiC	156.2
43	Fe$_3$O$_4$	197.02
44	Zincon–Si–MNPs	(84-104)
45	MoS$_2$	19.87
46	CeO$_2$	188.7
47	TiO$_2$	158.73
48	Fe$_3$O$_4$	82.64

TABLE 4: Continued.

S. no	Adsorbent	Adsorption
49	Oval CuO	125
50	Cluster CuO	116
51	Leaves CuO	117
52	Rod CuO	120
53	Nanosheet CuO	115
54	Present study (ZnO rods)	142

adsorbent surface. After the attainment of the stability, the rate of sequestration did not change for later contact time. This is due to the coverage of all the active moieties on the surface [32]. Therefore, no significant increase in sequestration is observed. The present experiment revealed that the equilibrium was attained within 30 min, which revealed excellent efficiency of ZnO-NR for the elimination of lead ions.

For the kinetic study, three (intraparticle diffusion, pseudo-second, and pseudo-first) models were computed. The expression for the pseudo-first-order is expressed in the following [33, 34]

$$\ln (q_e - q_t) = \ln q_e - k_1 t, \tag{7}$$

where k_1 is the rate constant, q_e is the equilibrium lead ions conc., and q_t is the lead ions at time t. The values of k_1 and q_e can be estimated using slope and intercept ($\ln (q_e - q_t)$ vs t). The MacKay and Ho model (pseudo-second-order) is depicted in the following [35]

$$\frac{t}{q_t} = \frac{1}{k_2 q_e^2} + \frac{1}{q_e} t, \tag{8}$$

where k_2 is rate constant and the initial sorption rate (h) is expressed by the following:

$$h = k_2 q_e^2. \tag{9}$$

Thus, h and q_e express the sorption rate and capacity at equilibrium, respectively. We can calculate the rate constant (k_2) using slope and intercept (t/q_t against t). The computed kinetic factors are depicted in Table 2 (Figures 14 and 15).

Based on the results and the correlation coefficients, it is inferred that the pseudo-second-order described the lead ion sequestration. The q_e (exp and cal) coincides well in the case of pseudo-second-order, which validates this model fitness for sequestration of lead ions on ZnO-NR. This model presumed that the elimination of lead ions onto ZnO-NR indicates the chemisorption [36].

3.4.1. Intraparticle Diffusion. The intraparticle diffusion model relation is presented as follows [37]

$$q_t = k_{id} \sqrt{t} + C, \tag{10}$$

where k_{id} and C are presenting the intraparticle diffusion rate constant and intercept, respectively. The sequestration

of lead ions from a bulk solution to solid surface occurred in multiple steps. Initially, the ions are adsorbed on the surface (film diffusion), and then ions are transferred within the pores (intraparticle diffusion). In batch mode, the possibility of intraparticle diffusion as a rate-determining step is enhanced under rapid stirring conditions. This model is valid if a plot of q_t versus $t^{1/2}$ furnished a straight line that passes through the origin. We found a deviation from a straight line (Figure 16), which reveals the rate-determining step as film diffusion. Data revealed that the intraparticle diffusion is unable to follow the lead ion sequestration onto ZnO-NR.

3.5. Thermodynamic Analysis. The influence of temperature on the sequestration of lead ions on ZnO-NR was scrutinized in the 293-323 K range. It can be seen that the rise in temperature leads to enhanced percent elimination efficiency of the lead ions. The lead ions adsorbed onto ZnO-NR while adsorbing heat, which revealed the endothermic sequestration process. This trend can be explained as; when the temperature is increased, the mobility of metal ions increased, this increased mobility results in effective interaction between lead ions and ZnO-NR, which helps in the elimination of metal ions. The thermodynamic variables, i.e., $\Delta G\circ$, $\Delta H\circ$, and $\Delta S\circ$ are designed using the relations shown in the following:

$$\Delta G\circ = -RT \ln K_C,$$
$$K_D = \frac{C_{As}}{C_e},$$
$$\ln K_D = \frac{\Delta S\circ}{R} - \frac{\Delta H\circ}{RT}, \quad (11)$$

where R, C_{As}, K_D, and T are gas constant, solid phase concentration (equilibrium), constant, and temperature (K), respectively. A plot of $1/T$ versus $\ln k_D$ (Figure 17) was utilized for $\Delta H\circ$ and $\Delta S\circ$ value computation. Table 3 depicts values for $\Delta G\circ$, $\Delta H\circ$, and $\Delta S\circ$. The positive values $\Delta S\circ$ is an indication of feasible sequestration of lead ions on to ZnO-NR. It also exhibited some interactions between sorbent and sorbate. The $\Delta H\circ$ (positive) is presenting the endothermic lead ion elimination for ZnO-NR and negative value $\Delta G\circ$ validate the spontaneous and feasible of the process. A comparative analysis of nanoadsorbents and nanocomposites for the sequestration of lead ions is depicted in Table 4. The nanoadsorbents showed promising efficiency for the sequestration of lead ions. Also, the ZnO-NR furnished auspicious efficacy for the sequestration of lead ions, which could possibly be employed for the remediation of lead ions in effluents. The higher efficiency of nanoadsorbents and nanocomposites could be due to the enhanced surface area and physicochemical properties versus the native adsorbents employed for lead ion sequestration [5, 38].

4. Conclusions

ZnO-NR was prepared through the hydrothermal method by employing CTAB as a surface-directing agent. The pre-pared ZnO-NR showed promising efficiency for the elimination of lead ions. The maximum removal was obtained at pH 6-7, ZnO-NR dosage of 0.06 g, initial concentration of lead ions of 25 mg/L, and agitation speed of 200 rpm and 323 K. The lead ion adsorption data fitted well to the Langmuir and pseudo-second-order kinetic models. The highest uptake capacity calculated from Langmuir's isotherm is 142 mg/g. The endothermic, spontaneous, and feasible lead ion sequestration using ZnO-NR was observed. Hence, the ZnO-NR can be utilized as an adsorbent to remediate metal ions in the effluents.

Data Availability

Data will be made available on request.

Conflicts of Interest

The authors declare that they have no conflicts of interest.

Acknowledgments

References

[1] R. Mohammed, M. E. M. Ali, E. Gomaa, and M. Mohsen, "Green ZnO nanorod material for dye degradation and detoxification of pharmaceutical wastes in water," *Journal of Environmental Chemical Engineering*, vol. 8, no. 5, article 104295, 2020.

[2] M. Mohsin, I. A. Bhatti, A. Ashar et al., "Fe/ fabrication for the enhanced photocatalytic performance under solar light irradiation for dye degradation," *Journal of Materials Research and Technology*, vol. 9, no. 3, pp. 4218–4229, 2020.

[3] D. Sachan, A. Ramesh, and G. Das, "Green synthesis of silica nanoparticles from leaf biomass and its application to remove heavy metals from synthetic wastewater: a comparative analysis," *Environmental Nanotechnology, Monitoring & Management*, vol. 16, article 100467, 2021.

[4] M. A. Ansari, M. Murali, D. Prasad et al., "Cinnamomum verum bark extract mediated green synthesis of ZnO nanoparticles and their antibacterial potentiality," *Biomolecules*, vol. 10, no. 2, p. 336, 2020.

[5] A. M. Awwad, M. W. Amer, and M. M. Al-Aqarbeh, "TiO$_2$-kaolinite nanocomposite prepared from the Jordanian kaolin clay: adsorption and thermodynamic of Pb(II) and cd(II) ions in aqueous solution," *Chemistry International*, vol. 6, no. 4, pp. 168–178, 2020.

[6] N. Oussama, H. Bouabdesselam, N. Ghaffour, and L. Abdelkader, "Characterization of seawater reverse osmosis fouled membranes from large scale commercial desalination plant," *Chemistry International*, vol. 5, no. 2, pp. 158–167, 2019.

[7] N. Benabdallah, D. Harrache, A. Mir, M. De La Guardia, and F. Benhachem, "Bioaccumulation of trace metals by red alga Corallina elongata in the coast of Beni Saf, west coast, Algeria," *Chemistry International*, vol. 3, no. 3, pp. 220–231, 2017.

[8] C. P. Ukpaka and O. N. Eno, "Modeling of Azadirachta indica leaves powder efficiency for the remediation of soil contaminated with crude oil," *Chemistry International*, vol. 7, no. 1, pp. 62–70, 2020.

[9] A. Kausar, K. Naeem, T. Hussain et al., "Preparation and characterization of chitosan/clay composite for direct rose FRN dye removal from aqueous media: comparison of linear and non-linear regression methods," *Journal of Materials Research and Technology*, vol. 8, no. 1, pp. 1161–1174, 2019.

[10] N. Alwadai, M. A. Haque, S. Mitra et al., "High-performance ultraviolet-to-infrared broadband perovskite photodetectors achieved via inter-/intraband transitions," *ACS Applied Materials & Interfaces*, vol. 9, no. 43, pp. 37832–37838, 2017.

[11] N. Alwadai, I. A. Ajia, B. Janjua et al., "Catalyst-free vertical ZnO-nanotube array grown on p-GaN for UV-light-emitting devices," *ACS Applied Materials & Interfaces*, vol. 11, no. 31, pp. 27989–27996, 2019.

[12] F. Majid, A. Nazir, S. Ata et al., "Effect of hydrothermal reaction time on electrical, structural and magnetic properties of cobalt ferrite," *Zeitschrift für Physikalische Chemie*, vol. 234, no. 2, pp. 323–353, 2020.

[13] A. Moulahi, F. Sediri, and N. Gharbi, "Hydrothermal synthesis of nanostructured zinc oxide and study of their optical properties," *Materials Research Bulletin*, vol. 47, no. 3, pp. 667–671, 2012.

[14] H. A. Shindy, M. A. El-Maghraby, and F. M. Eissa, "Solvatochromism and halochromism of some furo/pyrazole cyanine dyes," *Chemistry International*, vol. 7, no. 1, pp. 39–52, 2021.

[15] A. K. Zak, M. E. Abrishami, W. A. Majid, R. Yousefi, and S. Hosseini, "Effects of annealing temperature on some structural and optical properties of ZnO nanoparticles prepared by a modified sol-gel combustion method," *Ceramics International*, vol. 37, no. 1, pp. 393–398, 2011.

[16] P. Kumbhakar, D. Singh, C. Tiwary, and A. Mitra, "Chemical synthesis and visible photoluminescence emission from monodispersed ZnO nanoparticles," *Chalcogenide Letters*, vol. 5, no. 12, pp. 387–394, 2008.

[17] M. D. A. Sanda, M. Badu, J. A. Awudza, and N. O. Boadi, "Development of TiO$_2$-based dye-sensitized solar cells using natural dyes extracted from some plant-based materials," *Chemistry International*, vol. 7, no. 1, pp. 9–20, 2021.

[18] B. M. Amos-Tautua, O. Fakayode, S. P. Songca, and S. O. Oluwafemi, "Synthesis, spectroscopic characterization and singlet oxygen generation of 5,10,15,20-tetrakis(3,5-dimethoxyphenyl) porphyrin as a potential photosensitizer for photodynamic therapy," *Chemistry International*, vol. 5, pp. 10–15, 2020.

[19] B. Wei, K. Zheng, Y. Ji, Y. Zhang, Z. Zhang, and X. Han, "Size-dependent bandgap modulation of ZnO nanowires by tensile strain," *Nano Letters*, vol. 12, no. 9, pp. 4595–4599, 2012.

[20] M. W. Shammout and A. M. Awwad, "A novel route for the synthesis of copper oxide nanoparticles using bougainvillea plant flowers extract and antifungal activity evaluation," *Chemistry International*, vol. 7, no. 1, pp. 71–78, 2021.

[21] M. W. Amer and A. M. Awwad, "Green synthesis of copper nanoparticles by *Citrus limon* fruits extract, characterization and antibacterial activity," *Chemistry International*, vol. 7, no. 1, pp. 1–8, 2021.

[22] A. M. Awwad, M. W. Amer, N. M. Salem, and A. O. Abdeen, "Green synthesis of zinc oxide nanoparticles (ZnO-NPs) using Ailanthus altissima fruit extracts and antibacterial activity," *Chemistry International*, vol. 6, no. 3, pp. 151–159, 2020.

[23] R. Perveen, S. Shujaat, Z. Qureshi, S. Nawaz, M. I. Khan, and M. Iqbal, "Green versus sol-gel synthesis of ZnO nanoparticles and antimicrobial activity evaluation against panel of pathogens," *Journal of Materials Research and Technology*, vol. 9, no. 4, pp. 7817–7827, 2020.

[24] T. U. D. Thi, T. T. Nguyen, Y. D. Thi, K. H. T. Thi, B. T. Phan, and K. N. Pham, "Green synthesis of ZnO nanoparticles using orange fruit peel extract for antibacterial activities," *RSC Advances*, vol. 10, no. 40, pp. 23899–23907, 2020.

[25] K. K. Korir, E. M. Benecha, F. O. Nyamwala, and E. B. Lombardi, "Tuning electronic structure of ZnO nanowires via 3d transition metal dopants for improved photo-electrochemical water splitting: an *ab initio* study," *Materials Today Communications*, vol. 26, article 101929, 2021.

[26] A. M. Awwad, M. W. Amer, and M. M. Al-aqarbeh, "TiO2-kaolinite nanocomposite prepared from the Jordanian kaolin clay: adsorption and thermodynamics of Pb (II) and cd (II) ions in aqueous solution," *Chemistry International*, vol. 6, no. 4, pp. 168–178, 2020.

[27] A. M. Alkherraz, A. K. Ali, and K. M. Elsherif, "Removal of Pb (II), Zn (II), Cu (II) and Cd (II) from aqueous solutions by adsorption onto olive branches activated carbon: equilibrium and thermodynamic studies," *Chemistry International*, vol. 6, no. 1, pp. 11–20, 2020.

[28] I. Langmuir, "The adsorption of gases on plane surfaces of glass, mica and platinum," *Journal of the American Chemical Society*, vol. 40, no. 9, pp. 1361–1403, 1918.

[29] G. Mckay, H. Blair, and J. Gardner, "Adsorption of dyes on chitin. I. Equilibrium studies," *Journal of Applied Polymer Science*, vol. 27, no. 8, pp. 3043–3057, 1982.

[30] H. Freundlich and A. Seal, "Ueber einige Eigenschaften des Rhodanions," *Colloid & Polymer Science*, vol. 11, no. 6, pp. 257–263, 1912.

[31] M. Y. Kim, J. Y. Hwang, A. Mirzaei et al., "NO$_2$ gas sensing properties of ag-functionalized porous ZnO sheets," *Adsorption Science & Technology*, vol. 2023, article 9021169, 12 pages, 2023.

[32] R. N. P. Teixeira, V. O. S. Neto, J. T. Oliveira et al., "Removal of toxic metal ions from aqueous solutions in integrated clay adsorption and electroflotation," *Adsorption Science & Technology*, vol. 2022, article 3669652, 16 pages, 2022.

[33] S. Lagergren, "About the theory of so-called adsorption of soluble substances," *Sven Vetenskapsakad Handingarl*, vol. 24, pp. 1–39, 1898.

[34] Y. Ho and G. McKay, "The sorption of lead(II) ions on peat," *Water Research*, vol. 33, no. 2, pp. 578–584, 1999.

[35] Y. Ho and G. McKay, "Competitive sorption of copper and nickel ions from aqueous solution using peat," *Adsorption*, vol. 5, no. 4, pp. 409–417, 1999.

[36] S. Noreen, G. Mustafa, S. M. Ibrahim et al., "Iron oxide (Fe$_2$O$_3$) prepared via green route and adsorption efficiency evaluation for an anionic dye: kinetics, isotherms and thermodynamics studies," *Journal of Materials Research and Technology*, vol. 9, no. 3, pp. 4206–4217, 2020.

[37] W. J. Weber and J. C. Morris, "Kinetics of adsorption on carbon from solution," *Journal of the Sanitary Engineering Division*, vol. 89, no. 2, pp. 31–59, 1963.

[38] A. Babarinde and G. O. Onyiaocha, "Equilibrium sorption of divalent metal ions onto groundnut (Arachis hypogaea) shell: kinetics, isotherm and thermodynamics," *Chemistry International*, vol. 2, no. 3, pp. 37–46, 2016.